

Supporting Information

Designing an Improved Transition Metal Phosphide Catalyst for Hydrogen Evolution using Experimental and Theoretical Trends

Jakob Kibsgaard^{1,2}, Charlie Tsai^{1,2}, Karen Chan^{1,2}, Jesse D. Benck¹, Jens K. Nørskov^{1,2}, Frank Abild-Pedersen^{2,†} and Thomas F. Jaramillo^{1,2,‡}

¹ SUNCAT Center for Interface Science and Catalysis, Department of Chemical Engineering, Stanford University, Stanford, California, 94305, USA

² SUNCAT Center for Interface Science and Catalysis, SLAC National Accelerator Laboratory, 2575 Sand Hill Road, Menlo Park, California, 94025, USA

† F.A.-P.: abild@slac.stanford.edu

‡ T.F.J.: jaramillo@stanford.edu

Preparation of transition metal phosphide (TMP) working electrodes.

The as-prepared TMP Ti-foil supported samples were attached to a polyvinyl chloride-coated Cu wire placed inside a glass Pasteur pipette. Two-part epoxy was then used to insulate all of the conductive surfaces except for the TMP decorated side of the Ti foil. After epoxy masking, the exposed geometric areas of the TMP working electrodes were ~0.17-0.19 cm².

Lattice constant for Fe_{0.5}Co_{0.5}P.

The lattice constants for CoP, FeP and Fe_{0.5}Co_{0.5}P can be calculated based on relationship between d-spacing and lattice constants for an orthorhombic crystal system:

$$d_{hkl} = \frac{\lambda}{2 \sin(\theta_{hkl})} = \left[\frac{h^2}{a^2} + \frac{k^2}{b^2} + \frac{l^2}{c^2} \right]^{-1/2}$$

Solving the three coupled equations for the (011), (122) and (211) peaks gives the lattice constants shown in Table S1. The lattice constants for Fe_{0.5}Co_{0.5}P are in between

Table S1. (011), (122) and (211) peak positions and lattice constants for FeP, Fe_{0.5}Co_{0.5}P and CoP as determined by XRD.

	2θ ₀₁₁ [°]	2θ ₁₁₂ [°]	2θ ₂₁₁ [°]	a [Å]	b [Å]	c [Å]
FeP	32.71	46.29	48.31	5.19	3.10*	5.79*
Fe _{0.5} Co _{0.5} P	31.90	46.20	48.27	5.09	3.23	5.66
CoP	31.63	46.23	48.18	5.07	3.27	5.60

* since CoP and FeP have orthorhombic crystal systems, we have reversed *b* and *c* for FeP relative to reference ¹ to keep the crystal axes in this table consistent.

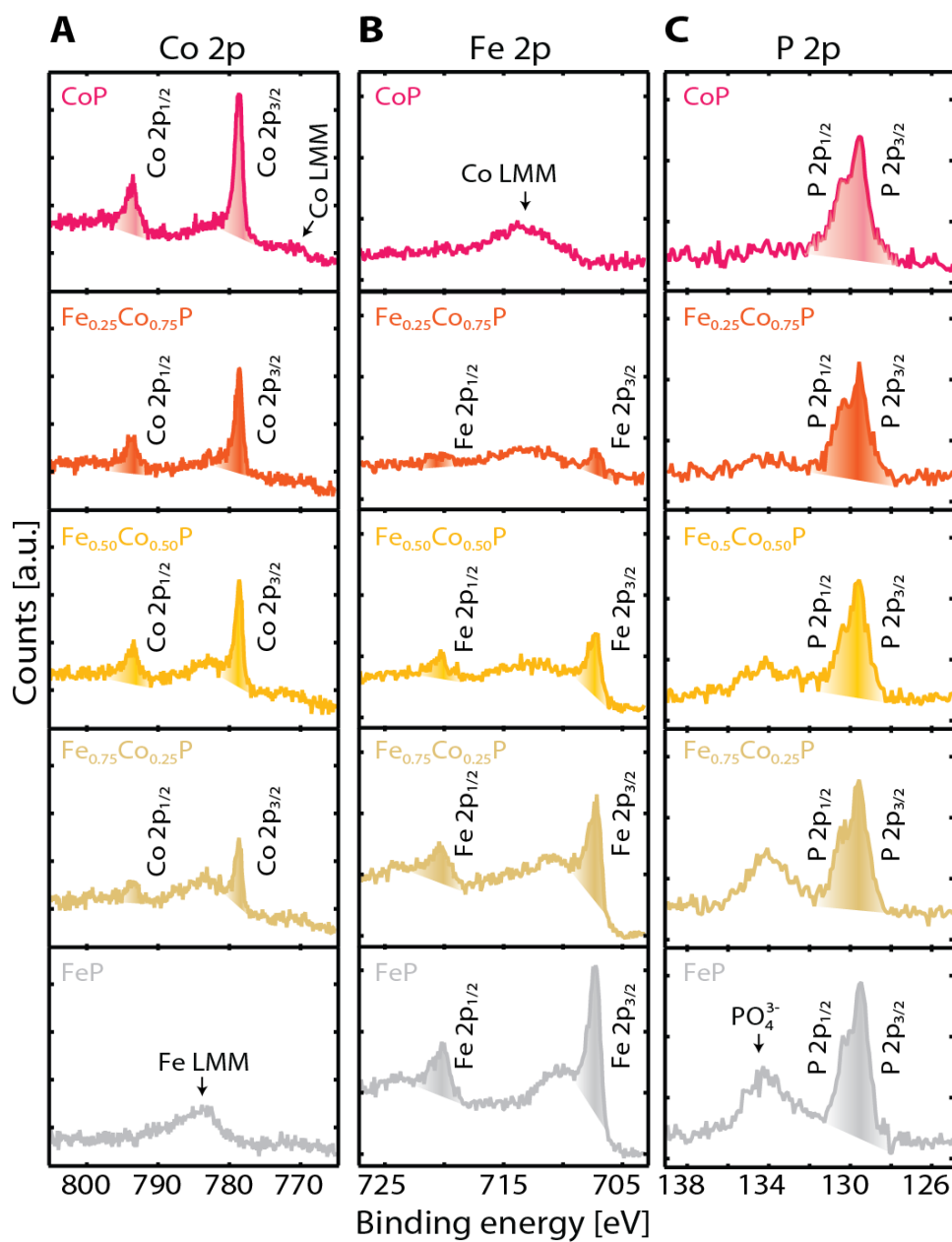


Figure S1. XPS spectra CoP, Fe_{0.25}Co_{0.75}P, Fe_{0.5}Co_{0.5}P, Fe_{0.75}Co_{0.25}P and FeP. (A) The Co 2p region indicates a cobalt phosphide in the case of the CoP, Fe_{0.25}Co_{0.75}P, Fe_{0.5}Co_{0.5}P and Fe_{0.75}Co_{0.25}P. (B) The Fe 2p region indicates an iron phosphide in the case of the FeP, Fe_{0.25}Co_{0.75}P, Fe_{0.5}Co_{0.5}P and Fe_{0.75}Co_{0.25}P. (C) The predominant doublet found in the P 2p region can be assigned to P bonded to a metal (i.e., phosphide).

Electrochemical active surface area.

Electrochemical capacitance measurements were used to determine the active surface area of each catalyst. To measure the electrochemical capacitance, the potential was swept between 0.10 to 0.30 V vs RHE five times at each of eleven different scan rates (10, 20, 40, 60, 80, 100, 120, 160, 200, 250 and 300 mV/s). The cyclic voltammograms can be seen in Figures S2A for a representative CoP electrode. We measured the capacitive currents in a potential range where no faradaic processes are observed, i.e. at 0.20 V vs. RHE. The measured capacitive currents are plotted as a function of scan rate in Figure S2B and a linear fit determined the specific capacitance to be $448 \mu\text{F cm}^{-2}$. The specific capacitance can be converted into an electrochemical active surface area (ECSA) using the specific capacitance value for a flat standard with 1 cm^2 of real surface area. The specific capacitance for a flat surface is generally found to be in the range of $20\text{-}60 \mu\text{F cm}^{-2}$.²⁻⁵ In the following calculations of TOF we assume $40 \mu\text{F cm}^{-2}$.

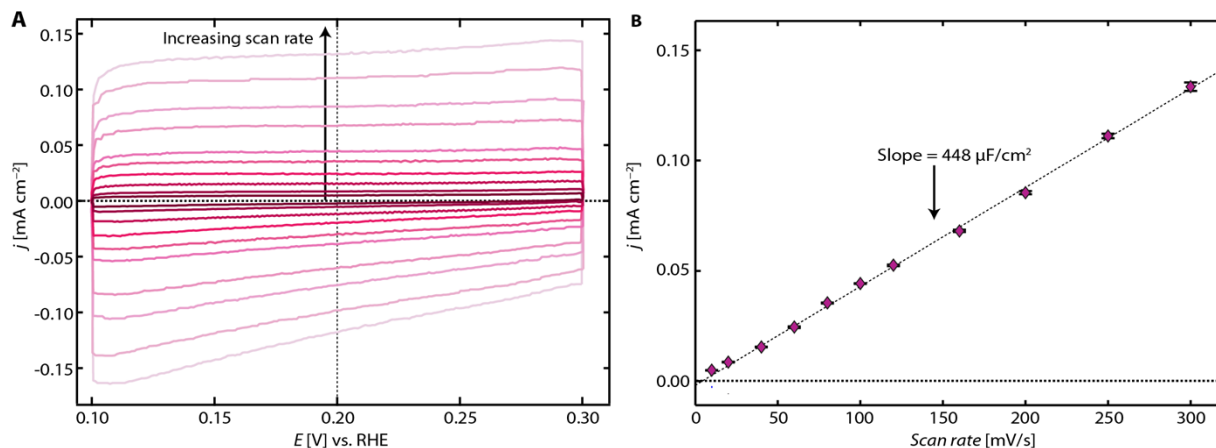


Figure S2. Electrochemical capacitance measurements to determine the surface area of a CoP electrode. (A) The capacitive current from double layer charging can be measured from cyclic voltammograms in a potential range where no Faradaic processes are observed. The capacitive currents were measured at 0.20 V vs RHE. (B) The measured capacitive currents plotted as a function of scan rate.

Calculated electrochemical active surface area.

$$A_{\text{ECSA}}^{\text{CoP}} = \frac{448 \mu\text{F cm}^{-2}}{40 \mu\text{F cm}^{-2} \text{ per cm}^2_{\text{ECSA}}} = 11.2 \text{ cm}^2_{\text{ECSA}}$$

Turnover frequency calculations.

To calculate the per-site turnover frequency (TOF), we used the following formula:

$$\text{TOF} = \frac{\# \text{ total hydrogen turn overs} / \text{cm}^2 \text{ geometric area}}{\# \text{ surface sites} / \text{cm}^2 \text{ geometric area}}$$

The total number of hydrogen turn overs was calculated from the current density according to:^{5, 6}

$$\#_{\text{H}_2} = \left(j \frac{\text{mA}}{\text{cm}^2} \right) \left(\frac{1 \text{C s}^{-1}}{1000 \text{mA}} \right) \left(\frac{1 \text{mol e}^-}{96485.3 \text{C}} \right) \left(\frac{1 \text{mol H}_2}{2 \text{mol e}^-} \right) \left(\frac{6.022 \times 10^{23} \text{H}_2 \text{ molecules}}{1 \text{mol H}_2} \right) = 3.12 \times 10^{15} \frac{\text{H}_2/\text{s}}{\text{cm}^2} \text{ per } \frac{\text{mA}}{\text{cm}^2}$$

Since the exact hydrogen binding sites are not known, we conservatively estimate the number of active sites as the total number of surface sites (including both the transition metal and P atoms as possible active sites) from the roughness factor together with the unit cell of the TMP. A similar approach was used to estimate TOF for Ni₂P,⁷ CoP,⁸ and MoP.⁹

surface sites per real surface area (here calculated for CoP):

$$\#_{\text{surface sites}} = \left(\frac{4 \text{ atoms / unit cell}}{93.07 \text{ \AA}^3 / \text{unit cell}} \right)^{\frac{2}{3}} = 1.948 \times 10^{15} \text{ atoms cm}^{-2}_{\text{real}}$$

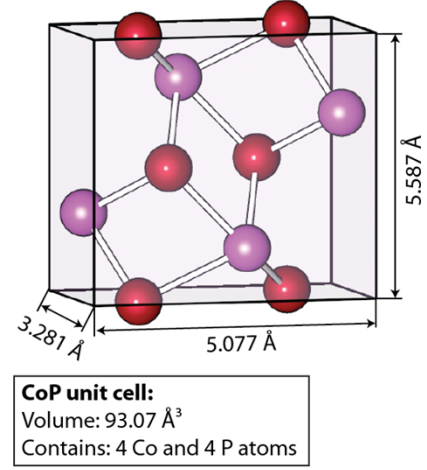


Figure S3. CoP unit cell. Co atoms: red and P atoms: purple.

Similar for the other TMP we find (for Fe_{0.25}Co_{0.75}P, Fe_{0.5}Co_{0.5}P and Fe_{0.75}Co_{0.25}P we took the weighted average of CoP and FeP):

Table S2. The volume of the unit cell and number of atoms contained in the unit cell are used to calculate the number of surface sites per surface area for the different TMPs.

	Unit cell volume [Å ³]	Atoms per unit cell	# Surface sites [atoms cm ⁻² _{real}]
MoP (and MoP S)	28.69	2	1.694 × 10 ¹⁵
FeP	93.21	8	1.946 × 10 ¹⁵
Fe ₂ P	102.81	9	1.972 × 10 ¹⁵
CoP	93.07	8	1.948 × 10 ¹⁵
Co ₂ P	132.48	12	2.017 × 10 ¹⁵
Ni ₂ P	100.54	9	2.001 × 10 ¹⁵
Fe _{0.25} Co _{0.75} P	93.11	8	1.947 × 10 ¹⁵
Fe _{0.5} Co _{0.5} P	93.14	8	1.947 × 10 ¹⁵
Fe _{0.75} Co _{0.25} P	93.18	8	1.946 × 10 ¹⁵

Finally, plot of current density can be converted into a TOF plot according to:

$$\text{TOF} = \frac{\left(3.12 \times 10^{15} \frac{\text{H}_2/\text{s}}{\text{cm}^2} \text{ per } \frac{\text{mA}}{\text{cm}^2} \right) \times |j|}{\#_{\text{surface sites}} \times A_{\text{ECSA}}}$$

Calculation details

All structures and electronic energies were calculated using plane-wave density functional theory (DFT) employing ultrasoft-pseudopotentials. The Quantum ESPRESSO code¹⁰ and the BEEF-vdW exchange correlation functional¹¹⁻¹³ were used with a plane wave cutoff and density cutoff of at

least 500 eV and 5000 eV respectively. For Fe containing structures, a higher plane wave cutoff was 800 eV and the density cutoff was 8000 eV in order to ensure proper convergence of the adsorption energies. At least three layers were used with the top layer allowed to relax. Periodic boundary conditions with dipole corrections were used in all cases, with at least 10 Å of vacuum in the z -direction to separate neighboring slabs. All calculations except that for MoP were calculated with spin-polarization. The structures were relaxed until the total forces on each atom were less than 0.05 eV/Å. The calculated lattice parameters are shown in Table S3. And the results agree very well with experimentally determined quantities. The hydrogen adsorption free energy ΔG_H was calculated as in previous studies.

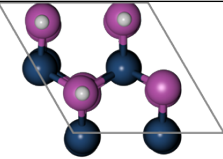
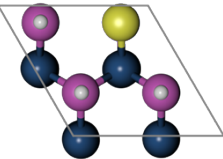
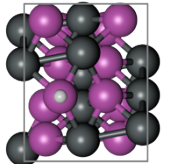
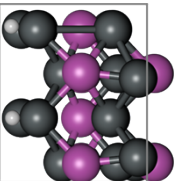
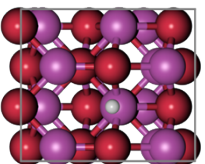
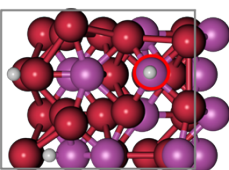
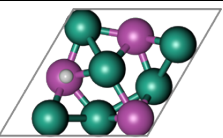
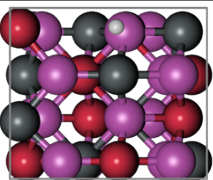
As a first approximation, the stable surfaces for each TMP were estimated using the Bravais-Friedel-Donnay-Harker (BFDH) crystal morphology algorithm.¹⁴ Although this method is based purely on geometry, it proved remarkably successful in a previous study on cobalt oxides, where the estimated stable surfaces were confirmed by explicit calculations of the surface energies.¹⁵ Among the surfaces estimated to be present, 2~5 surfaces of each TMP were taken and the ΔG_H was calculated for hydrogen coverages from $\theta_H = 0$ ML to 1 ML. Here, the hydrogen coverage θ_H is defined as the fraction of a monolayer with respect to the number of active sites on the surface. The number of active sites on the surface is defined as number of possible sites where hydrogen can adsorb at a reasonable binding energy ($\Delta G_H < 0.7$ eV). The coverage at which hydrogen desorption becomes more favorable than further adsorption is taken to be the coverage where HER occurs. For each TMP, the surface with the most thermoneutral ΔG_H was considered to be the most active amongst the stable surfaces; the ΔG_H at this surface is thus taken to be the descriptor for that TMP. The differential hydrogen adsorption free energies were calculated as in previous studies.^{16, 17} The relevant active surfaces are shown in Table S4 with the ΔG_H of the final adsorbed hydrogen at the steady-state coverage. In the case of molybdenum phosphosulfide (MoP|S) the $\frac{1}{4}$ of the phosphorous atoms was substituted with a sulfur atom. This sulfur coverage was previously found by XPS for MoP|S.⁹

Table S3. Transition metal phosphide compounds, their structures, and their lattice parameters; theoretical and experimental lattice parameters are in close agreement.

Compound	Space Group	Lattice parameters [Å]						
		Theoretical			Experimental			
		a	b	c	a	b	c	Ref.
MoP	$P\bar{6}2$ $O\{6\}E$ $rror!m$ 2	3.245	3.244	3.200	3.230	3.230	3.200	Schönberg et. al. ¹⁸
FeP	Pna21	5.156	5.762	3.052	5.193	5.792	3.099	Elsukov et. al. ¹
Fe ₂ P	$P\bar{6}2$ $O\{6\}E$ $rror!m$	5.815	5.815	3.423	5.868	5.868	3.458	Carlsson et. al. ¹⁹
CoP	Pnma	5.076	3.269	5.537	5.077	3.281	5.587	Rundqvist et. al. ²⁰
Co ₂ P	Pnma	5.526	3.508	6.605	5.649	3.513	6.607	Skála et. al. ²¹
Ni ₂ P	$P\bar{6}2$	5.895	5.895	3.379	5.859	5.859	3.382	Larson et. al. ²²

$\text{Fe}_{0.5}\text{Co}_{0.5}\text{P}$	$\text{O}\{6\}$ rror! Pnma	5.039	3.226	5.618	5.09	3.23	5.670	Selte et. al. ²³
--	---	-------	-------	-------	------	------	-------	-----------------------------

Table S4. The most active surfaces amongst the most likely surfaces as estimated using the BFDH algorithm; their surface structures, steady-state hydrogen coverages, and hydrogen adsorption free energies with the relative errors are listed. The lines represent the repeating unit cells and atoms in purple are phosphorous, atoms in white are hydrogen, and the remaining ones correspond to the metals, as shown in the main text. Where there is ambiguity, the active hydrogen is circled in red.

Compound	Surface	Structure	Site	θ_{H} [ML]	ΔG_{H} [eV]	Rel. Error [eV]
MoP	(001)		P	0.75	-0.166	-
MoP S	(001)		P	1.0	0.048	0.015
FeP	(011)		P	0.25	0.133	0.094
Fe ₂ P	(100)		Fe-bridge	0.50	-0.123	0.024
CoP	(101)		Co-bridge	0.25	-0.085	0.047
Co ₂ P	(101)		P	0.75	0.212	0.024
Ni ₂ P	(001)		Ni-hollow	0.33	0.138	0.064
Fe _{0.5} Co _{0.5} P	(101)		Fe-Co-bridge	0.25	0.004	0.029

References

1. E. P. Elsukov, Y. N. Vorobev, A. V. Trubachev and V. A. Barinov, *Phys. Status Solidi A*, 1990, **117**, 291-298.
2. D. C. Grahame, *Chem. Rev.*, 1947, **41**, 441-501.
3. R. Kötz and M. Carlen, *Electrochim. Acta*, 2000, **45**, 2483-2498.
4. B. E. Conway and B. V. Tilak, *Electrochim. Acta*, 2002, **47**, 3571-3594.
5. J. D. Benck, Z. B. Chen, L. Y. Kuritzky, A. J. Forman and T. F. Jaramillo, *ACS Catal.*, 2012, **2**, 1916-1923.
6. Z. Chen, D. Cummins, B. N. Reinecke, E. Clark, M. K. Sunkara and T. F. Jaramillo, *Nano Lett.*, 2011, **11**, 4168-4175.
7. E. J. Popczun, J. R. McKone, C. G. Read, A. J. Biacchi, A. M. Wiltrout, N. S. Lewis and R. E. Schaak, *J. Am. Chem. Soc.*, 2013, **135**, 9267-9270.
8. E. J. Popczun, C. G. Read, C. W. Roske, N. S. Lewis and R. E. Schaak, *Angew. Chem.*, 2014, **53**, 5427-5430.
9. J. Kibsgaard and T. F. Jaramillo, *Angew. Chem. Int. Ed.*, 2014, **53**, 14433-14437.
10. G. Paolo, B. Stefano, B. Nicola, C. Matteo, C. Roberto, C. Carlo, C. Davide, L. C. Guido, C. Matteo, D. Ismaila, C. Andrea Dal, G. Stefano de, F. Stefano, F. Guido, G. Ralph, G. Uwe, G. Christos, K. Anton, L. Michele, M.-S. Layla, M. Nicola, M. Francesco, M. Riccardo, P. Stefano, P. Alfredo, P. Lorenzo, S. Carlo, S. Sandro, S. Gabriele, P. S. Ari, S. Alexander, U. Paolo and M. W. Renata, *J. Phys.: Condens. Matter*, 2009, **21**, 395502.
11. J. Wellendorff, K. T. Lundgaard, A. Møgelhøj, V. Petzold, D. D. Landis, J. K. Nørskov, T. Bligaard and K. W. Jacobsen, *Phys. Rev. B*, 2012, **85**, 235149.
12. M. Dion, H. Rydberg, E. Schröder, D. C. Langreth and B. I. Lundqvist, *Phys. Rev. Lett.*, 2004, **92**, 246401.
13. D. C. Langreth, B. I. Lundqvist, S. D. Chakarova-Käck, V. R. Cooper, M. Dion, P. Hyldgaard, A. Kelkkanen, J. Kleis, K. Lingzhu, L. Shen, P. G. Moses, E. Murray, A. Puzder, H. Rydberg, E. Schröder and T. Thonhauser, *J. Phys.: Condens. Matter*, 2009, **21**, 084203.
14. R. Docherty, G. Clydesdale, K. J. Roberts and P. Bennema, *J. Phys. D: Appl. Phys.*, 1991, **24**, 89-99.
15. M. Bajdich, M. Garcia-Mota, A. Vojvodic, J. K. Nørskov and A. T. Bell, *J. Am. Chem. Soc.*, 2013, **135**, 13521-13530.
16. B. Hinnemann, J. K. Nørskov and H. Topsøe, *J. Phys. Chem. B*, 2004, **109**, 2245-2253.
17. C. Tsai, F. Abild-Pedersen and J. K. Nørskov, *Nano Lett.*, 2014, **14**, 1381-1387.
18. N. Schönberg, *Acta Chem. Scand.*, 1954, **8**, 226-239.
19. B. Carlsson, M. Gölin and S. Rundqvist, *J. Solid State Chem.*, 1973, **8**, 57-67.
20. Rundqvist, S. and P. C. Nawapong, *Acta Chem. Scand.*, 1965, **19**, 1006-&.
21. R. Skála and M. Drábek, *Bulletin of Geosciences*, 2001, **76**, 209 - 216.
22. E. Larsson, *Ark. Kemi*, 1965, **23**, 335-365.
23. K. Selte, L. Birkeland and A. Kjekshus, *Acta Chem. Scand.*, 1978, **32a**, 731-735.